JASA ARTICLE

Acoustic feedback path modeling for hearing aids: Comparison of physical position based and position independent models

Tobias Sankowsky-Rothe,[1,a)] Henning Schepker,[2] Simon Doclo,[2] and Matthias Blau[3]
[1]*Institut für Hörtechnik und Audiologie, Jade Hochschule, D-26121 Oldenburg, Germany*
[2]*Signal Processing Group, Department of Medical Physics and Acoustics, and Cluster of Excellence Hearing4All, University of Oldenburg, D-26111 Oldenburg, Germany*
[3]*Institut für Hörtechnik und Audiologie, and Cluster of Excellence Hearing4All, Jade Hochschule, D-26121 Oldenburg, Germany*

ABSTRACT:
Acoustic feedback in hearing aids occurs due to the coupling between the hearing aid loudspeaker and microphones. In order to reduce acoustic feedback, adaptive filters are often used to estimate the feedback path. To increase the convergence speed and decrease the computational complexity of the adaptive algorithms, it has been proposed to split the acoustic feedback path into a time-invariant fixed part and a time-varying variable part. A key question of this approach is how to determine the fixed part. In this paper, two approaches are investigated: (1) a digital filter design approach that makes use of the signals of at least two hearing aid microphones and (2) a defined physical location approach using an electro-acoustic model and the signals of one hearing aid microphone and an additional ear canal microphone. An experimental comparison using measured acoustic feedback paths showed that both approaches enable one to reduce the number of variable part coefficients. It is shown that individualization of the fixed part increases the performance. Furthermore, the two approaches offer solutions for different requirements on the effort to a specific hearing aid design on the one hand and the effort during the hearing aid fitting on the other hand. *© 2020 Author(s). All article content, except where otherwise noted, is licensed under a Creative Commons Attribution (CC BY) license (http://creativecommons.org/licenses/by/4.0/).* https://doi.org/10.1121/10.0000509
(Received 18 July 2019; revised 9 December 2019; accepted 10 December 2019; published online 16 January 2020)
[Editor: James F. Lynch] Pages: 85–100

I. INTRODUCTION

In recent years the number of hearing-impaired persons supplied with open-fitting hearing aids has been steadily increasing. Open-fitting hearing aids usually comprise a behind-the-ear (BTE) unit with two or three microphones. In this work we additionally consider the availability of an ear-canal microphone as depicted in Fig. 1(a). While open-fitting hearing aids largely alleviate problems related to the occlusion effect (i.e., the perception of one's own voice), they are especially prone to the problem of acoustic feedback (Blau *et al.*, 2008). This requires the development of fast-acting and robust acoustic feedback cancellation algorithms.

By definition, the term *acoustic feedback path* describes the acoustic path from output of the receiver to input of the microphone. However, it is common practice to use this term with transductions from and to electrical signals included, i.e., the path from electrical receiver input to electrical microphone output. This path is still referred to as acoustic path in order to distinguish it from other feedback paths which may exist, e.g., a mechanical path.

Among several different strategies to reduce the acoustic feedback in hearing aids (see, e.g., Guo *et al.*, 2012; Nakagawa *et al.*, 2015; Schepker *et al.*, 2016; Spriet *et al.*, 2008; van Waterschoot and Moonen, 2011), adaptive feedback cancellation (AFC) is the most promising approach. In AFC the impulse response (IR) of the acoustic feedback path between the hearing aid receiver and the microphone is estimated using an adaptive filter, theoretically allowing for perfect cancellation of the feedback signal. In general, the convergence speed and computational complexity of the adaptive filter depend on the number of adaptive parameters (Sayed, 2003). In order to reduce the number of adaptive parameters, it has been proposed to decompose the acoustic feedback path into two filters (Kates, 2000; Ma *et al.*, 2011; Schepker and Doclo, 2014): (1) a time-invariant *fixed part* and (2) a time varying *variable part*. While the fixed part models components that can be assumed, for one individual subject, to be the same in many feedback paths, e.g., intra-individual transducer characteristics and individual ear canal geometries, the time-varying variable part allows one to track changes of the acoustic feedback path caused, e.g., by a moving telephone. In this paper we consider modeling of both transducer characteristics and individual ear canal geometries using the fixed part.

This decomposition can be achieved by means of different approaches, e.g., using electro-acoustic modeling (Egolf *et al.*, 1989; Egolf *et al.*, 1985; Kates, 1988) or using different optimization procedures for digital filter design (Giri and Zhang, 2017; Hashemgeloogerdi and Bocko, 2018; Ma *et al.*, 2011; Schepker and Doclo, 2015, 2016a,b). In electro-acoustic models the different parts of the acoustic

[a)]Electronic mail: tobias.sankowsky@jade-hs.de

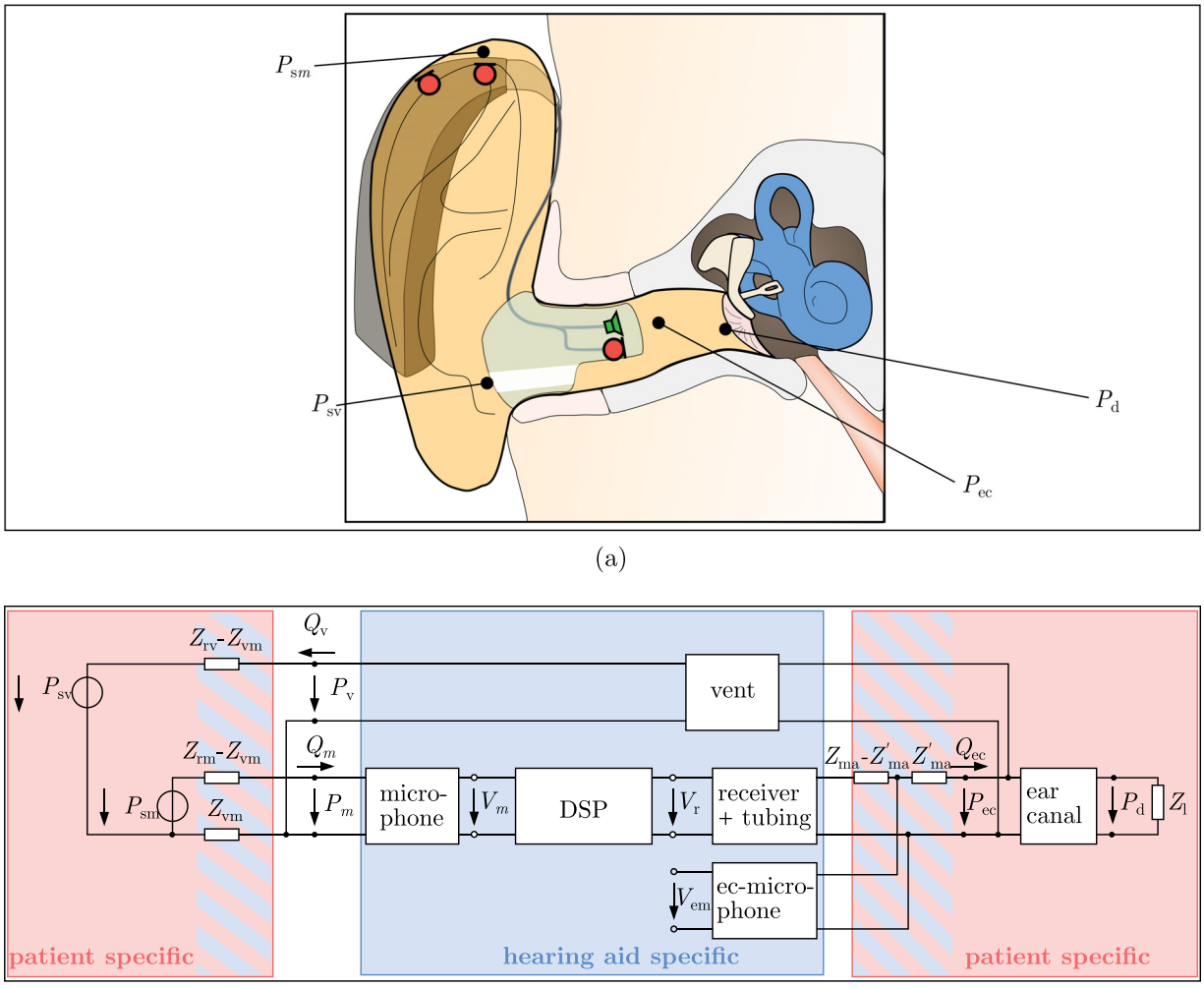

FIG. 1. (Color online) (a) Sketch of the scenario with the hearing aid attached to the ear. (b) Electro-acoustic model of the hearing aid at the ear based on the model shown in Blau *et al.* (2009).

feedback path, e.g., the transducer, the tubing, the ear-drum, and ear canal as well as the venting are modeled separately. Using two-ports to characterize each of these parts and connecting them in chain they can be used to, e.g., determine the howling frequency components (Egolf *et al.*, 1989). Furthermore, electro-acoustic models can be used to assess the sensitivity of the feedback paths to changes of the ear canal and venting geometries (Kates, 1988). Models based on digital filter design aim at finding a set of common filter coefficients that optimize either the least-squares error (Giri and Zhang, 2017; Hashemgeloogerdi and Bocko, 2018; Ma *et al.*, 2011; Schepker and Doclo, 2016b) or the maximum stable gain of the hearing aid (Schepker and Doclo, 2015, 2016a). While these models do not relate the fixed part to the underlying physical and electro-acoustic properties of the feedback path, they have been shown to be successful in reducing the number of variable part parameters and improving the performance of a state-of-the-art AFC algorithm (Schepker and Doclo, 2016a,b).

Nevertheless, in order to provide a meaningful interpretation of the fixed part it is desirable to specify the physical location up to which the acoustic feedback path can be assumed to be time-invariant. Using electro-acoustic models of the acoustic feedback path allows one to separate the complete acoustic feedback path into meaningful units. Such models can be used to specify the physical location between the fixed and the variable feedback path.

In this paper we first briefly review an existing acoustic feedback path model based on digital filter design (Schepker and Doclo, 2016b). Second, in order to define a specific physical location where the fixed part ends, we propose a novel electro-acoustic model of the acoustic feedback path that exploits the availability of an ear canal microphone. Since electro-acoustic analogies are typically not very well suited to model the complex and potentially time-varying sound field outside the ear canal, we also propose to use an all-zero filter to model the variable part. Third, although the ear canal microphone is not placed at

https://doi.org/10.1121/10.0000509

the same physical location where the acoustic feedback path is assumed to be split, we propose to directly use the ear canal microphone to measure the fixed part and model it using digital filter optimization. Thus defining the physical location allows one to directly control the physical parameters that contribute to the fixed part of the acoustic feedback path and allows it to in addition take advantage of the high modeling accuracy of digital filter design and possibilities to track changes.

This paper is organized as follows. In Sec. II the generic acoustic feedback cancellation scenario and the acoustic feedback path decomposition is introduced. In Sec. III the three different feedback path models, i.e., the feedback path model based on digital filter design, the feedback path model based on electro-acoustic modeling, and a novel combination of these two, are described. In Sec. IV the three feedback path models are compared using measured acoustic feedback paths from a two-microphone behind-the-ear hearing aid. In Sec. V the results are discussed.

II. SCENARIO

Consider the single-microphone-single-loudspeaker acoustic feedback cancellation scenario depicted in Fig. 2(a). The incoming signal in the hearing aid microphone in the frequency-domain is denoted as $S_m(e^{j\Omega})$ at normalized frequency Ω. The microphone signal $Y_m(e^{j\Omega})$ is processed by the hearing aid gain function $G(e^{j\Omega})$, generating the loudspeaker signal $X(e^{j\Omega})$. The loudspeaker and the microphone are coupled by the acoustic feedback path $H_m(e^{j\Omega})$ and the hearing aid gain function $G(e^{j\Omega})$. An (adaptive) filter $\hat{H}_m(e^{j\Omega})$ is used to remove an estimate $\hat{F}_m(e^{j\Omega})$ of the feedback signal $F_m(e^{j\Omega}) = H_m(e^{j\Omega})X(e^{j\Omega})$ from the microphone signal, yielding the error signal $E_m(e^{j\Omega})$. In order to reduce the number of parameters of the filter $\hat{H}_m(e^{j\Omega})$ approximating the acoustic feedback path, the decomposition shown in Fig. 2(b) can be used, where

$$H_m(e^{j\Omega}) \approx \hat{H}_m(e^{j\Omega}) = \hat{H}^f(e^{j\Omega})\hat{H}^v_m(e^{j\Omega}). \tag{1}$$

In this equation, $\hat{H}^f(e^{j\Omega})$ is the time-invariant fixed part independent of $H_m(e^{j\Omega})$ and $\hat{H}^v_m(e^{j\Omega})$ is the variable part that depends on the $H_m(e^{j\Omega})$. In the following we will omit the frequency dependency for conciseness whenever possible.

III. FEEDBACK PATH MODELS

As mentioned above, the feedback path can be modeled using different approaches that allow for the decomposition of the acoustic feedback path according to Eq. (1). In the following the acoustic feedback path models based on digital filter design (DFD), the acoustic feedback path model based on electro-acoustic modeling as well as a combination of both will be described. While the feedback path model based on DFD requires the measurement of multiple acoustic feedback paths, e.g., at different microphone locations of the BTE unit, the acoustic feedback path models based on a defined physical location (DPL) for the decomposition (i.e., the electro-acoustic and the combined model) make use of an ear canal microphone to estimate the fixed part of the acoustic feedback path.

A. Feedback path model based on digital filter design

The goal of the feedback path model based on digital filter design (Schepker and Doclo, 2016b) is to decompose a set of M measured acoustic feedback paths $H_m(e^{j\Omega})$ of length N^h_z depicted in Fig. 3(a) into a fixed pole-zero filter $\hat{H}^f(e^{j\Omega})$ with N^f_p poles and N^f_z zeros and M variable all-zero filters $\hat{H}^v_m(e^{j\Omega})$ with N^v_z zeros each depicted in Fig. 3(b), i.e.,

$$\hat{H}^f(e^{j\Omega}) = \frac{B^f(e^{j\Omega})}{A^f(e^{j\Omega})} = \frac{\sum_{i=0}^{N^f_z} b^f[i]e^{-ji\Omega}}{1 + \sum_{i=1}^{N^f_p} a^f[i]e^{-ji\Omega}}, \tag{2}$$

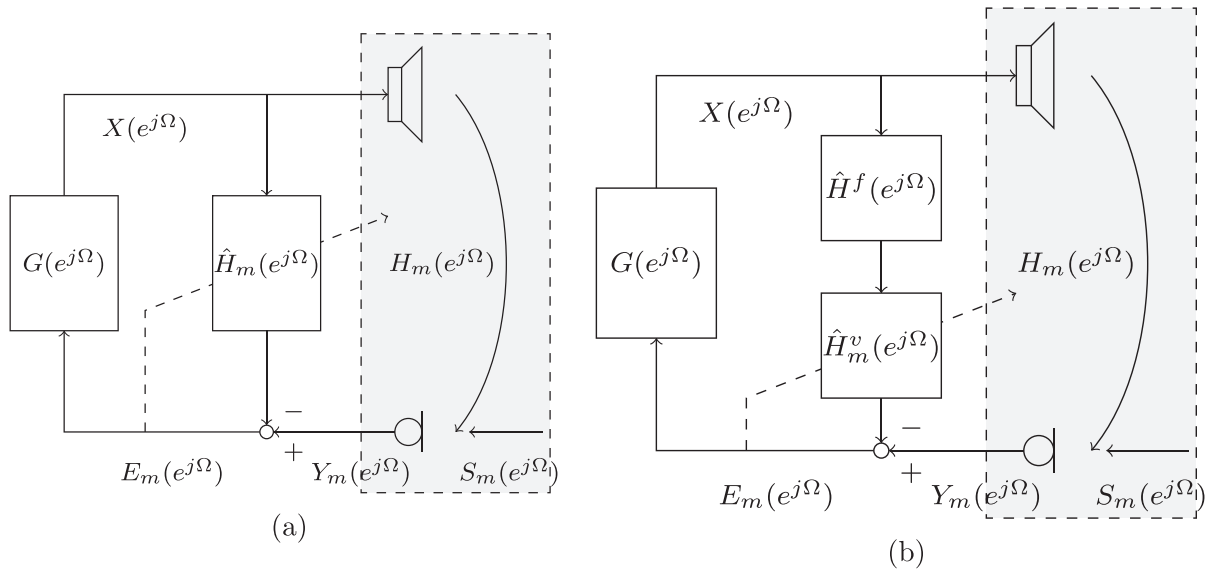

FIG. 2. Acoustic feedback cancellation frameworks using (a) a conventional adaptive feedback canceller and (b) an adaptive feedback canceller using the proposed feedback path decomposition. The grey box indicates the components included in the acoustic feedback path.

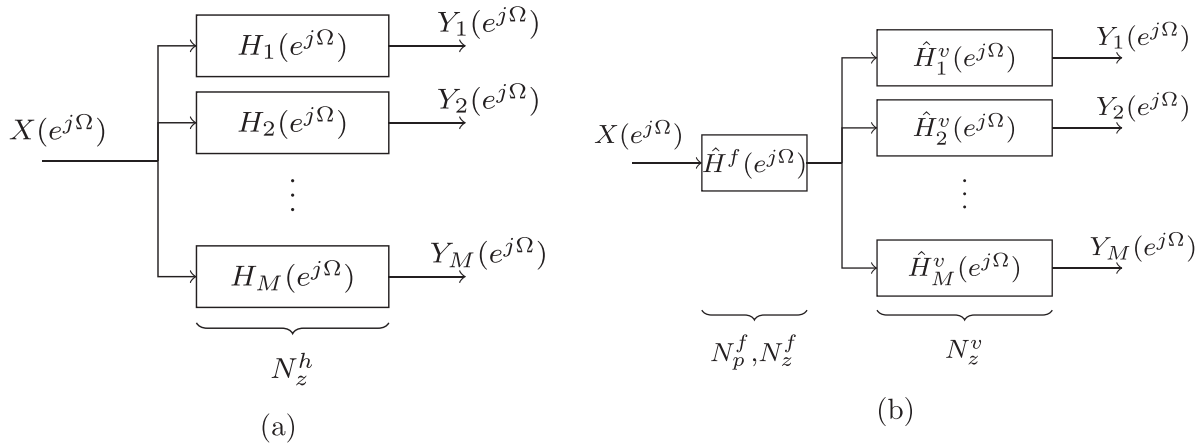

FIG. 3. System models for the digital filter design based feedback path model: (a) general SIMO system and (b) approximation of the SIMO system using a fixed part.

$$\hat{H}_m^v(e^{j\Omega}) = B_m^v(e^{j\Omega}) = \sum_{i=0}^{N_z^v} b_m^v[i]e^{-ji\Omega}, \tag{3}$$

where $b^f[i]$, $a^f[i]$, and $b_m^v[i]$ are the coefficients of the polynomials representing the fixed zeros, fixed poles, and variable zeros, respectively. Note that $A^f(e^{j\Omega})$ is assumed to be based on a monic polynomial, i.e., $a^f[0] = 1$. Note that the feedback path model based on digital filter design does not make any assumptions on the specific components of the acoustic feedback path that are part of the fixed part but aims at including all components that are common across multiple feedback paths. In order to estimate all the coefficients of the fixed part and the variable parts, the aim is to minimize the least-squares cost function

$$J_{OE}(\mathbf{a}^f, \mathbf{b}^f, \mathbf{b}^v) = \sum_{m=1}^{M} \int_0^{\pi} |\tilde{E}_m(e^{j\Omega})|^2 d\Omega, \tag{4}$$

with $\tilde{E}_m(e^{j\Omega})$ the so-called output-error

$$\tilde{E}_m = H_m - \frac{B^f}{A^f} B_m^v, \tag{5}$$

and $\mathbf{a}^f = [a^f[1]\, a^f[2] \cdots a^f[N_p^f]]^T$, $\mathbf{b}^f = [b^c[0]\, b^f[1] \cdots b^f[N_z^f]]^T$, $\mathbf{b}^v = [(\mathbf{b}_1^v)^T\, (\mathbf{b}_2^v)^T \cdots (\mathbf{b}_M^v)^T]^T$, and $\mathbf{b}_m^v = [b_m^v[0]\, b_m^v[1] \cdots b_m^v[N_z^v]]^T$ the coefficient vectors of the fixed poles, fixed zeros, the stacked variable zeros, and the microphone dependent variable zeros, respectively. $[\cdot]^T$ denotes the transpose operation.

The output-error in Eq. (5) is non-linear in A^f, B^f, and B_m^v, and hence minimization of the cost function in Eq. (4) is not straightforward. In order to circumvent this difficulty, Schepker and Doclo (2016b) proposed to minimize the so-called equation-error instead, i.e., to minimize the least-squares cost function

$$J_{EE}(\mathbf{a}^f, \mathbf{b}^f, \mathbf{b}^v) = \sum_{m=1}^{M} \int_0^{\pi} |E_m(e^{j\Omega})|^2 d\Omega, \tag{6}$$

with E_m the equation-error

$$E_m = A^f H_m - B^f B_m^v. \tag{7}$$

The equation-error is only non-linear in B^f and B_m^v and can be optimized using a two-step alternating least-squares procedure (Schepker and Doclo, 2016b). Assuming the coefficient vectors of the fixed part fixed, in the first step the variable part coefficient vector minimizing Eq. (6) is computed. Assuming the coefficient vector of the variable part fixed, in the second step the fixed part coefficient vectors minimizing Eq. (6) are computed. These two steps are alternated until a convergence criterion is fulfilled. For a more detailed description of the optimization procedure the reader is referred to (Schepker and Doclo, 2016b). Note that the fixed pole-zero filter estimated by minimizing the equation-error is in general stable (Schepker and Doclo, 2016b). However, minimizing the equation-error cost function in Eq. (6) leads to an undesired weighting of the output-error in Eq. (5), i.e., $E_m = A^f \tilde{E}_m$, which may lead to poor modeling accuracy in the vicinity of large spectral resonances (Schepker and Doclo, 2016b). To counteract this inherent weighting, the so-called weighted equation-error can be iteratively minimized, i.e., at each iteration i the least-squares cost function

$$J_{WEE}(\mathbf{a}_i^f, \mathbf{b}_i^f, \mathbf{b}_i^v) = \sum_{m=1}^{M} \int_0^{\pi} \left| \frac{1}{A_{i-1}^f(e^{j\Omega})} E_{m,i}(e^{j\Omega}) \right|^2 d\Omega \tag{8}$$

is minimized (Schepker and Doclo, 2016b).

From Eq. (8) it can be observed that if $A_{i-1}^f \approx A_i^f$, then $(1/A_{i-1}^f)E_{m,i} \approx \tilde{E}_m$, hence approximating the desired output-error minimization in Eq. (4). However, note that the minimization in Eq. (8) does not guarantee stability of the estimated all-pole filter component $1/A^f(z)$, thus requiring a constraint on the pole location. Here we use a constraint based on the positive realness of the frequency response $A^f(e^{j\Omega})$ as proposed in Schepker and Doclo (2016b), i.e.,

$$\Re\{A_i^f(e^{j\Omega})\} \geq \delta \quad \forall\Omega, \tag{9}$$

https://doi.org/10.1121/10.0000509

where $\Re\{\cdot\}$ denotes the real part and δ is a small positive constant to control the stability constraint. Similar to minimizing Eq. (6), Eq. (8) subject to the constraint in Eq. (9) can be minimized using a two-step alternating least-squares procedure (Schepker and Doclo, 2016b).

B. Feedback path model based on electro-acoustic modeling

The electro-acoustic model of the hearing aid attached to the ear is depicted in Fig. 1(b). Based on that model, the components can be divided into three parts.

(1) Patient-specific parts, i.e., the sound field at the outer ear, the ear canal, and the load impedance Z_l including the eardrum with the attached middle ear.
(2) Hearing aid-specific parts, i.e., microphones, receiver with tubing, and the venting.
(3) Patient-specific and hearing aid-specific, i.e., the radiation impedances of the vent Z_rv and the microphone Z_{rm} as well as the transfer impedance Z_{vm} between the lateral end of the vent and the microphone, and the cross-sectional change between the receiver tubing and the ear canal represented by the impedance Z_ma.

Using this model, the acoustic feedback path is defined by

$$H_m = \frac{V_m}{V_\mathrm{r}}, \tag{10}$$

where V_m is the voltage at the microphone and V_r is the voltage at the receiver. In the original model depicted in Fig. 1, P_sv and P_{sm} are sound pressures from an external source at the rigidly terminated vent and at the rigidly terminated hearing aid microphone. In order to model the acoustic feedback path only, the model in Fig. 1(b) can by simplified by omitting the sound sources P_sv and P_{sm} outside the ear (i.e., $P_\mathrm{sv} = P_{sm} = 0$), reducing the two-port representing the ear canal and the load impedance to a lumped element Z_c, and by omitting the two-port representing the DSP resulting in an open loop structure as depicted in Fig. 4. Assuming the input impedance of the microphone to be high compared to the impedance of the sound field, i.e., assuming the volume velocity at the microphone Q_m and the lower row of the transfer matrix parameters to be zero, the only parameter used to characterize the microphone equals $1/B_m$, i.e., the reciprocal of the microphone sensitivity B_m. Note that due to the open loop structure the upper right transfer matrix parameter equals zero. Based on these assumptions the feedback path estimate is calculated as

$$\hat{H}_m = \frac{Q_\mathrm{s}}{V_\mathrm{r}} \frac{Z_\mathrm{s} Z_\mathrm{ec}}{Z_\mathrm{s} + Z_\mathrm{ec} + Z_\mathrm{ma}} Y_\mathrm{tv} Z_\mathrm{vm} B_m, \tag{11}$$

with volume velocity Q_s and impedance Z_s the parameters of the Norton-equivalent source, representing the receiver and tubing, Z_ec the ear canal impedance resulting from Z_c and the vent input impedance acting in parallel, and Y_tv the transfer admittance of the vent. Y_tv is defined as the ratio of the volume velocity at the output of the vent Q_v divided by the sound pressure at the input of the vent P_ec, i.e.,

$$Y_\mathrm{tv} = \frac{1}{v_{11} Z_\mathrm{rv} + v_{12}}, \tag{12}$$

with v_{11} and v_{12} the transfer matrix parameters which may be calculated based on a model of an acoustic duct (cf. Sec. III B 2).

If the sound pressure in the ear canal P_ec is known, the parameters of the Norton-equivalent source Q_s and Z_s as well as the input impedance of the ear canal Z_ec are not required and Eq. (11) can be reformulated as

$$\hat{H}_m = \frac{P_\mathrm{ec}}{V_\mathrm{r}} Y_\mathrm{tv} Z_\mathrm{vm} B_m. \tag{13}$$

In order to sense the sound pressure in the ear canal, we make use of an ear canal microphone which is located at the medial end of the hearing aid earmold. Unfortunately, this position is located at a cross-sectional change which is known to be influenced by near-field effects (see, e.g., Stinson and Daigle, 2007).

On the other hand, the geometry of this setup, including the position of the microphone, can be assumed to remain unchanged over time, and hence a simple way of accounting for near-field effects is to split Z_ma into two parts, $(Z_\mathrm{ma} - Z'_\mathrm{ma})$ and Z'_ma, see Figs. 5 and 1(b). Consequently, the sound pressure in the ear canal, P_ec, is related to the voltage at the ear canal microphone V_em by

$$P_\mathrm{ec} = \frac{V_\mathrm{em}}{B_\mathrm{em}} H_\mathrm{nf}, \tag{14}$$

with B_em the sensitivity of the ear canal microphone and

$$H_\mathrm{nf} = \left(\frac{Z'_\mathrm{ma}}{Z_\mathrm{ec}} + 1 \right)^{-1}, \tag{15}$$

the transfer function accounting for the near-field effects.

1. Decomposition of the feedback path model based on electro-acoustic modeling

Different factors influence the acoustic feedback path of a hearing aid. For example, variations of the acoustics

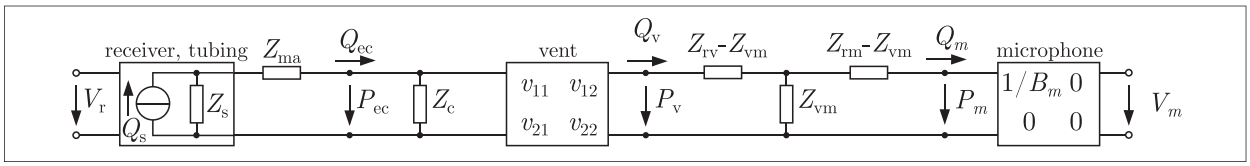

FIG. 4. Equivalent circuit of the feedback path.

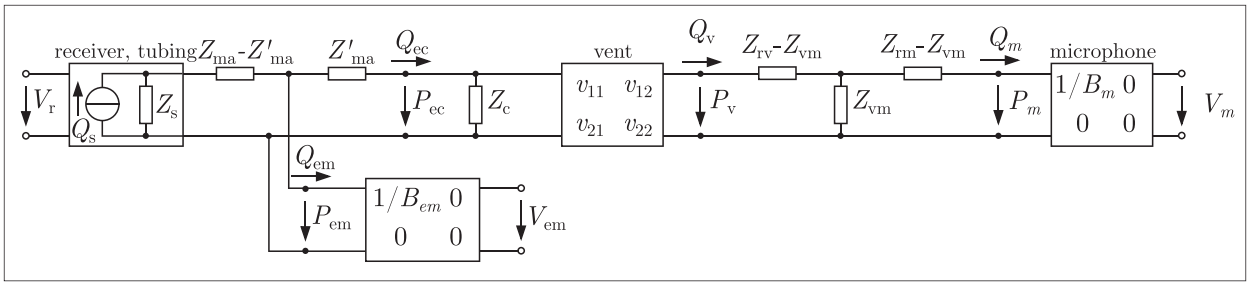

FIG. 5. Equivalent circuit of the feedback path with incorporation of an ear canal microphone.

outside the ear (Hellgren *et al.*, 1999) and ear-canal geometries (Sankowsky-Rothe *et al.*, 2015b) both have a large influence, while different jaw positions have only minor effects (Hellgren *et al.*, 1999; Sankowsky-Rothe and Blau, 2017). Motivated by these results, we propose to decompose the acoustic feedback path based on the different parts used in the model.

For an individually fitted hearing aid the size of the vent will not change and the dimensions of the ear canal undergo only small changes due to jaw movements. Therefore, it is reasonable to incorporate the characteristics of the receiver, the microphones, the ear canal and the vent into the highly individual but (mostly) time-invariant fixed part, i.e., decompose the acoustic feedback paths in Eq. (13) using Eq. (14) into a fixed part

$$\hat{H}^{\mathrm{f}} = \frac{V_{\mathrm{em}}}{V_{\mathrm{r}}} H_{\mathrm{nf}} Y_{\mathrm{tv}} \frac{B_m}{B_{\mathrm{em}}}, \tag{16}$$

and variable parts

$$\hat{H}_m^v = Z_{\mathrm{vm}} = \frac{P_m}{Q_{\mathrm{v}}}, \tag{17}$$

where the variable parts consider the acoustics of the outer sound field represented by the transfer impedance Z_{vm}, i.e., the sound pressure at the microphone relative to the volume velocity out of the lateral end of the vent.

Strictly speaking, every variation in the feedback path, including variations in the variable part, affects the fixed part as defined above, because the load impedance seen by the source varies. This includes variations in the acoustics of the outer sound field, and variations which are not explicitly included in the model, e.g., additional leakage due to a loose fit. For open fittings, which are addressed here, the effect on the load impedance is supposed to be small. In principle, any variation of the feedback path has to be compensated by the variable part.

2. Parameters of the feedback path model based on electro-acoustic modeling

The fixed part of the feedback path model according to Eq. (16) consists on the one hand of components being well suited for parametric electro-acoustic modeling, e.g., the near-field effects H_{nf} and the transfer admittance of the vent Y_{tv}. Other components cannot easily be modeled parametrically and are therefore measured, e.g., the transfer function of the voltage at the ear canal microphone relative to the voltage driving the receiver $V_{\mathrm{em}}/V_{\mathrm{r}}$, and the transfer function of the microphone sensitivities B_m/B_{em}. In the following, the computation of H_{nf} and Y_{tv} is described.

The near-field effects are characterized by a shift of the minima in the measured sound pressure (Sankowsky-Rothe *et al.*, 2015a). If near-field effects have a significant influence, the level of the transfer function V_{em}/V_m will show a characteristic notch followed by a peak and the phase shows an increase followed by a decrease, since the minimum is shifted only in V_{em} but not in V_m. This could potentially be used to estimate the transfer function $Z'_{\mathrm{ma}}/Z_{\mathrm{ec}}$ used to compute the transfer function H_{nf} accounting for the near-field effects. This transfer function can be described by four parameters: an acoustic mass M_{ma} representing the impedance Z_{ma}, and an acoustic mass M_{ec}, an acoustic compliance C_{ec}, and a resistance R_{ec} representing the impedance Z_{ec}.

Alternatively, the function used to compensate the near-field effects can be approximated by a pole-zero filter using a pair of complex conjugated poles and a pair of complex conjugated zeros. Since the absolute value of both the poles and the zeros can be assumed to be the same, only three parameters need to be estimated: the absolute value r, the phase angle of the poles φ_{p}, and the phase angle of the zeros φ_{z}. The transfer function H_{nf} is then given by

$$H_{\mathrm{nf}}(r, \varphi_{\mathrm{p}}, \varphi_{\mathrm{z}}) = \frac{1 - 2r\cos(\varphi_{\mathrm{z}})e^{-j\Omega} + r^2 e^{-j2\Omega}}{1 - 2r\cos(\varphi_{\mathrm{p}})e^{-j\Omega} + r^2 e^{-j2\Omega}}. \tag{18}$$

The three parameters were estimated as follows: In order to determine the phase angles of the poles and zeros, the frequencies at which the derivative of the unwrapped phase of the transfer function V_{em}/V_m had a minimum and a maximum, respectively, were identified, see Fig. 6(a). It should be noted that the acoustic feedback path as well as the sound pressure in the ear canal typically show a minimum between 4 and 10 kHz, which is in first approximation caused by a quarter wavelength resonance of the residual ear canal. Hence, in the identification only frequencies larger than 3 kHz were considered. The phase angles of the poles and zeros are given by the normalized frequencies $\varphi_{\mathrm{p}} = \Omega_{\mathrm{p}}$ and $\varphi_{\mathrm{z}} = \Omega_{\mathrm{z}}$, computed as

$$\Omega_{\mathrm{p}} = \mathrm{argmax}\left(\frac{d\,\mathrm{arg_u}\{V_{\mathrm{em}}/V_m\}}{d\Omega}\right), \tag{19}$$

https://doi.org/10.1121/10.0000509

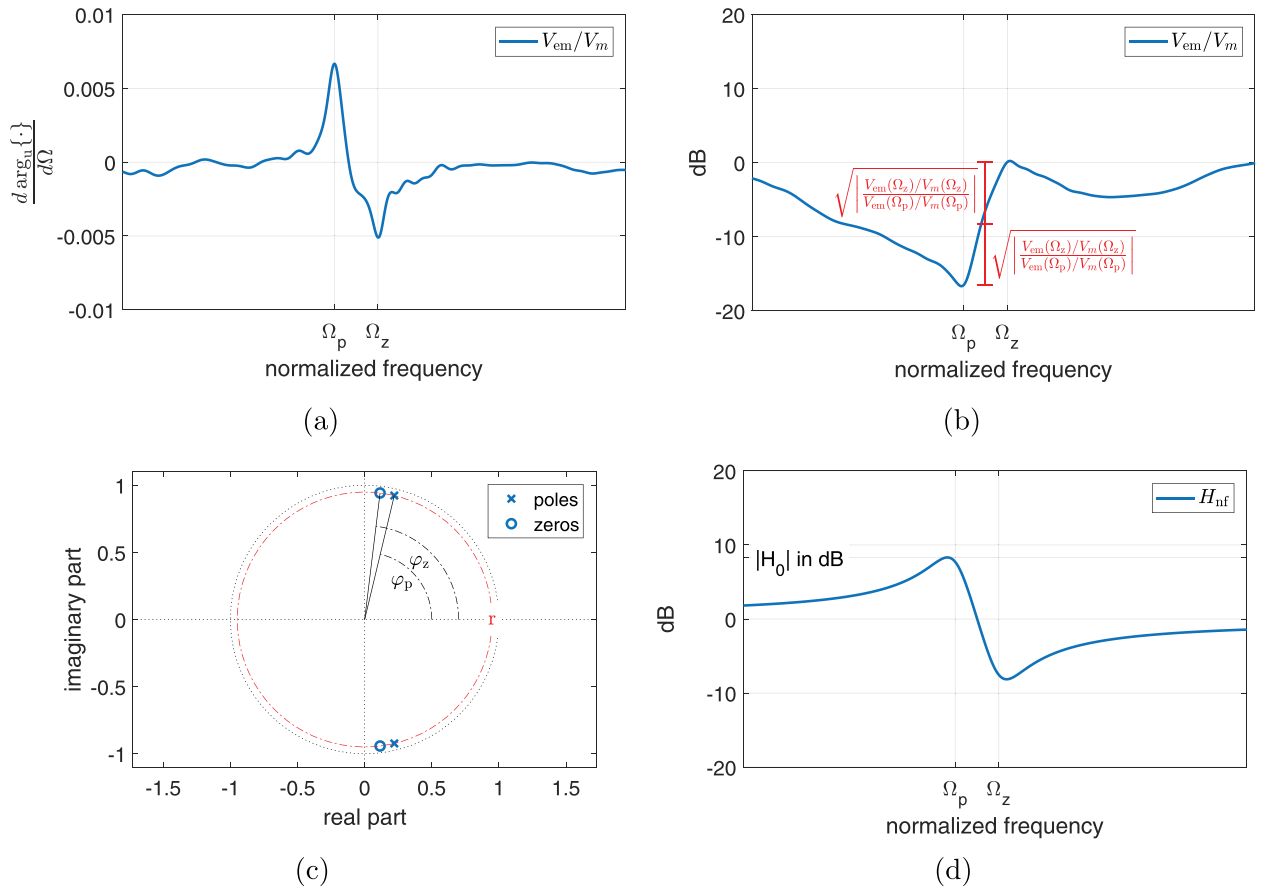

FIG. 6. (Color online) Parameter estimation of the transfer function H_{nf} used to compensate nearfield effects. (a) Phase angles φ_p and φ_z of the poles and zeros are derived from the derivative of the unwrapped phase of the transfer function V_{em}/V_m. (b) The magnitude $|H_{nf}(\Omega_p)|$ is determined from the transfer function V_{em}/V_m at frequencies Ω_p and Ω_z. (c) Poles and zeros in the z-plane. (d) Magnitude in dB of the resulting transfer function H_{nf}.

$$\Omega_z = \operatorname{argmin}\left(\frac{d\arg_u\{V_{em}/V_m\}}{d\Omega}\right), \tag{20}$$

with $\arg_u\{\cdot\}$ the unwrapped phase.

The transfer function H_{nf} used to compensate for the near-field effects is specified to have unity gain, i.e., the first polynomial coefficient representing the zeros $b[0] = 1$. Thus, the value of the transfer function at the frequency of the pole location is given by

$$H_{nf}(\Omega_p) = H_0 = \begin{cases} \sqrt{\left|\frac{V_{em}(\Omega_z)/V_m(\Omega_z)}{V_{em}(\Omega_p)/V_m(\Omega_p)}\right|}\, e^{-j\pi/4} & \text{if } \varphi_z > \varphi_p, \\ \sqrt{\left|\frac{V_{em}(\Omega_z)/V_m(\Omega_z)}{V_{em}(\Omega_p)/V_m(\Omega_p)}\right|}\, e^{j\pi/4} & \text{if } \varphi_z < \varphi_p, \end{cases} \tag{21}$$

with the magnitude determined as depicted in Fig. 6(b). Using Eq. (18) the absolute value of the poles and zeros [see Fig. 6(c)] can then be calculated by

$$r = \left| \sqrt{-e^{j2\varphi_p} + \left(\left(\cos\varphi_z - \cos\varphi_p H_0\right) \frac{e^{j\varphi_p}}{H_0 - 1} \right)^2} - \left(\cos\varphi_z - \cos\varphi_p H_0\right) \frac{e^{j\varphi_p}}{H_0 - 1} \right|. \tag{22}$$

The calculation of the transfer admittance Y_{tv} of the vent using Eq. (12) requires the transfer matrix parameters v_{11}, v_{12} and the radiation impedance Z_{rv} of the vent. The vent was modeled as an acoustical duct considering visco-thermal losses, according to Benade (1968). This model requires the length l_v and the radius a_v of the vent and additionally we consider a frequency-independent scalar damping factor g_v with which the real part of the propagation constant is multiplied. In previous tests, the coupling of the damping factor g_v to the radius using $g_v = 7$ mm/a_v turned out to be suitable.

The radiation impedance Z_{rv} was modeled as a piston in an infinite baffle with the following approximation [Strutt (Lord Rayleigh), 1896, p. 302]:

$$Z_{rv}(k, a_v) = \frac{\rho c}{\pi a_v^2}\left(\frac{(ka_v)^2}{2} + j\frac{8ka_v}{3\pi}\right), \tag{23}$$

with $k = 2\pi\Omega/c$ the wave number, ρ the density of air, and c the speed of sound.

For the transfer impedance Z_{vm} between the lateral end of the vent and the microphone free-field propagation is assumed, i.e., no additional obstructions are in proximity to the ear. Thus the distance-dependent transfer impedance was modeled as a point source on a baffle, i.e.,

$$Z_{\mathrm{vm}}(d_{\mathrm{vm}}) = e^{-jkd_{\mathrm{vm}}} \frac{j\Omega\rho}{2\pi d_{\mathrm{vm}}}, \tag{24}$$

with d_{vm} being the distance between the vent and the microphone.

The vent parameters and the distance between vent and microphone were estimated using a two-step procedure. In the first step, a desired transfer admittance $\tilde{Y}_{\mathrm{tv}}$ was computed from the measured transfer functions V_m/V_{em} and B_{em}/B_m, the correction for the near-field effects $H_{\mathrm{nf}}(r, \varphi_{\mathrm{p}}, \varphi_{\mathrm{z}})$, and the transfer impedance $Z_{\mathrm{vm}}(d_{\mathrm{vm}})$ with an initial value for the distance d_{vm}, using

$$\tilde{Y}_{\mathrm{tv}} = \frac{V_m}{V_{\mathrm{em}}} \frac{B_{\mathrm{em}}}{B_m} \frac{1}{H_{\mathrm{nf}} Z_{\mathrm{vm}}}. \tag{25}$$

The initial value of d_{vm} was assumed to be 3.8 cm, determined by a measurement of the distance at one ear. In order to obtain the parameters a_{v}, l_{v}, and g_{v} used to compute the transfer admittance Y_{tv} in Eq. (12), the cost function

$$J(a_{\mathrm{v}}, l_{\mathrm{v}}, g_{\mathrm{v}}) = \sum_n \left(\left(20 \log_{10} \left| \frac{Y_{\mathrm{tv}}(\Omega_n)}{\tilde{Y}_{\mathrm{tv}}(\Omega_n)} \right| \right)^2 \times \left(1 + \frac{\arg_{\mathrm{u}}(Y_{\mathrm{tv}}(\Omega_n)) - \arg_{\mathrm{u}}(\tilde{Y}_{\mathrm{tv}}(\Omega_n))}{2\pi} \right)^2 \right) \tag{26}$$

was minimized, using logarithmically spaced frequencies Ω_n from 0.0131 to 1.309 (corresponding to 100 Hz to 10 kHz at a sampling frequency of 48 kHz). Minimization of Eq. (26) is performed using a simplex-fitting procedure (fminsearch from MATLAB).

In the second step, the distance d_{vm} was estimated by minimizing the least-squares cost function

$$J(d_{\mathrm{vm}}) = \sum_n \left(\frac{\arg_{\mathrm{u}}\left(\frac{V_m}{V_{\mathrm{em}}} \frac{B_{\mathrm{em}}}{B_m} \frac{1}{H_{\mathrm{nf}}} \right) - \arg_{\mathrm{u}}(Y_{\mathrm{tv}} Z_{\mathrm{vm}})}{2\pi} \right)^2. \tag{27}$$

In order to avoid erroneous fitting using unreliable measurements, in both fitting procedures, only those frequency bins were considered where the magnitude squared coherence of V_{em} and V_{r} was at least 0.8.

The variable part in this modeling approach represents the acoustics outside the ear. A first approximation assuming free-field propagation for a static case is given by Eq. (24). A possible extension in order to consider reflecting obstructions near the ear would be to incorporate one or more image sources into the model. However, this kind of modeling is expected to lack sufficient precision required for acoustic feedback cancellation. Therefore, in Sec. III C we additionally propose to combine the fixed part as obtained from Eq. (16) with a variable part obtained using digital filter design.

3. Parameter reduction of measured transfer functions and model variants of the fixed part model based on electro-acoustic modeling

In the modeling approach presented above many components are modeled using electro-acoustic parametrization. However, the transfer functions $V_{\mathrm{em}}/V_{\mathrm{r}}$ and B_m/B_{em} are less suited for this kind of parametrization and measurements are usually required. Although this allows for a precise modeling, parametric modeling allows for a low number of parameters to describe these transfer functions efficiently. One way to reduce the number of parameters of the model components characterized by measured transfer functions is to represent the latter by pole-zero filters.

Two different variants to obtain a pole-zero filter for the fixed part, based on electro-acoustic modeling, are proposed.

(A) the product of the transfer functions $V_{\mathrm{em}}/V_{\mathrm{r}}$ and B_m/B_{em} is modeled using a pole-zero filter, i.e., the number of parameters $N^{f,A}$ is given by the sum of N_p^A poles, N_z^A zeros, and the six parameters (a_{v}, l_{v}, g_{v}, r, φ_{p}, φ_{z}) of the electro-acoustic parametrization, resulting in

$$\hat{H}^{f,A} = H_{\mathrm{nf}} Y_{\mathrm{tv}} \frac{\sum_{i=0}^{N_z^{f,A}} b^A[i] e^{-ij\Omega}}{1 + \sum_{i=1}^{N_p^{f,A}} a^A[i] e^{-ij\Omega}}, \tag{28}$$

with $b^A[i]$ and $a^A[i]$ the coefficients of the zeros and poles, respectively. Variant A results in a total number of $N^{f,A} = N_p^{f,A} + N_c^{f,A} + 6$ parameters.

(B) The complete fixed part obtained from Eq. (16) is modeled using a pole-zero filter, i.e.,

$$\hat{H}^{f,B} = \frac{\sum_{i=0}^{N_z^{f,B}} b^B[i] e^{-ij\Omega}}{1 + \sum_{i=1}^{N_p^{f,B}} a^B[i] e^{-ij\Omega}}, \tag{29}$$

with $b^B[i]$ and $a^B[i]$ the coefficients of the zeros and poles, respectively. Variant B results in a total number of $N^{f,B} = N_p^{f,B} + N_z^{f,B}$ parameters.

C. Combined feedback path model

1. Combined models using electro-acoustic modeling to derive the fixed part

In order to exploit the high robustness and generalization of electro-acoustic modeling as well as the high flexibility and fast adaptation of digital filter design, in this section both approaches are combined. The combined models using electro-acoustic modeling to derive the fixed part comprises the parametrized variants A or B of the fixed part presented

https://doi.org/10.1121/10.0000509

in Sec. III B 3 and a variable part modeled as an finite-impulse-response- (FIR-) filter, i.e.,

$$\hat{H}^v(z) = B^v(z) = \sum_{i=0}^{N_z^v} b^v[i] z^{-i}, \tag{30}$$

with N_z^v filter coefficients. The filter coefficients were estimated by minimizing the following least-squares cost function of the Wiener-Filter:

$$J(\mathbf{b}^v) = \int_0^\pi |H(e^{j\Omega}) - B^v(e^{j\Omega})\hat{H}^{f,x}(e^{j\Omega})|^2 d\Omega, \tag{31}$$

with $\hat{H}^{f,x}$ being either $\hat{H}^{f,A}$ or $\hat{H}^{f,B}$.

2. Combined model using a measured transfer function as the fixed part

While the fixed part can be modeled using electro-acoustic modeling as presented in Sec. III C 1, it could also be measured using a microphone placed at a position where the acoustic feedback path is time-invariant or only slowly time-varying. This can be assumed for the ear canal microphone, which could hence be exploited also to measure the fixed part of the acoustic feedback paths. Therefore, we propose a combined model $\hat{H}^{f,C}$ in which the product of the transfer functions $V_{\mathrm{em}}/V_{\mathrm{r}}$ and B_m/B_{em} is represented by a pole-zero filter with $N_p^{f,C}$ poles and $N_z^{f,C}$ zeros for the fixed part referred to variant C. The variable part was again modeled by a FIR-filter whose coefficients are obtained by minimizing Eq. (31) using $\hat{H}^{f,C}$.

IV. EXPERIMENTAL COMPARISON

A. Acoustic setup and performance measures

In this section, the different feedback path models, i.e., the model based on digital filter design (cf. Sec. III A), and the model based on a defined physical location (cf. Secs. III B and III C) including their different variants are compared using measured acoustic feedback paths. The measurements [published in Sankowsky-Rothe *et al.* (2015b)] were performed using a two-microphone BTE hearing aid attached to a dummy head with variable ear canals similar to Hiipakka *et al.* (2010). Different conditions for the acoustics outside the ear, the ear-canal geometries, and the venting were used. More specifically, three different conditions for the acoustics outside the ear were considered: (1) a free-field condition, i.e., without any obstruction in vicinity of the ear, (2) a wall condition, where the dummy head was placed with its shoulder at a wall, and (3) a telephone condition, where a telephone receiver was placed close to the ear. Furthermore, two different ear canal sizes were used, (1) a small ear canal of 6 mm diameter and 15 mm length and (2) a large ear canal of 7 mm diameter and 20 mm length. In all measurements custom made open-fitting ear molds were used. The measurements were performed at a sampling rate of 48 kHz and provided as transfer functions computed using a discrete Fourier transform with 2^{14} frequency points. The measured feedback paths for the different conditions and ear canal sizes used in the experimental evaluation are depicted in Fig. 7(a). For comparison $V_{\mathrm{em}}/V_{\mathrm{r}}$, which is the voltage at the ear canal microphone relative to the voltage at the receiver, is shown in Fig. 7(b).

The performance of the models is assessed using the added stable gain (ASG), which is defined as (Kates, 2001)

$$\mathrm{ASG} = \mathrm{MSG} - 20\log_{10}\left(\min_\Omega \frac{1}{|H(e^{j\Omega})|}\right), \tag{32}$$

where MSG denotes the maximum stable gain defined as

$$\mathrm{MSG} = 20\log_{10}\left(\min_\Omega \frac{1}{|H(e^{j\Omega}) - \hat{H}(e^{j\Omega})|}\right). \tag{33}$$

B. Algorithmic parameters

The algorithmic parameters used in the experimental evaluation will be described in the following. First, the general parameters are considered followed by the parameters of the feedback path models based on digital filter design and the parameters of the feedback path models based on a defined physical location for the decomposition.

1. General parameters

All impulse responses were computed from the transfer functions as provided in (Sankowsky-Rothe *et al.*, 2015b), resampled to 16 kHz, and truncated to a length of 100 samples.

2. Parameters of the feedback path model based on digital filter design

The feedback path model based on digital filter design obtained by minimizing the equation-error (ee) cost functions in Eq. (6) and the weighted equation-error (wee) cost function in Eq. (8) was computed for the following set of fixed poles, fixed zeros, and variable zeros: $N_p^c, N_z^c \in [0, 1, 2, \ldots, 30]$, $N_z^v \in [0, 2, 4, \ldots, 50]$. The frequency response $A_i^f(e^{j\Omega})$ in Eq. (9) of the poles of the fixed part used in the constraint when minimizing the weighted equation-error in Eq. (8) was computed using a 2048-point discrete Fourier transform. Convergence of the alternating least-squares procedures was assumed when the normalized sum of the difference between successive common part coefficient vectors and successive variable part coefficients vectors was smaller than a predefined constant ϵ, i.e.,

$$\frac{||\mathbf{p}_{i-1}^c - \mathbf{p}_i^c||_2}{||\mathbf{p}_{i-1}^c||_2} + \frac{||\mathbf{b}_{i-1}^v - \mathbf{b}_i^v||_2}{||\mathbf{b}_{i-1}^v||_2} \leq \epsilon \tag{34}$$

with $\mathbf{p}_i^c = [\,(\mathbf{a}_i^c)^T \quad (\mathbf{b}_i^c)^T\,]^T$ and $\epsilon = 10^{-4}$. Furthermore, for the minimization of the weighted equation error minimization $\delta = 10^{-4}$ was chosen in Eq. (9). Two different sets of acoustic feedback paths were considered to compute the fixed pole-zero filter: (1) only the acoustic feedback paths

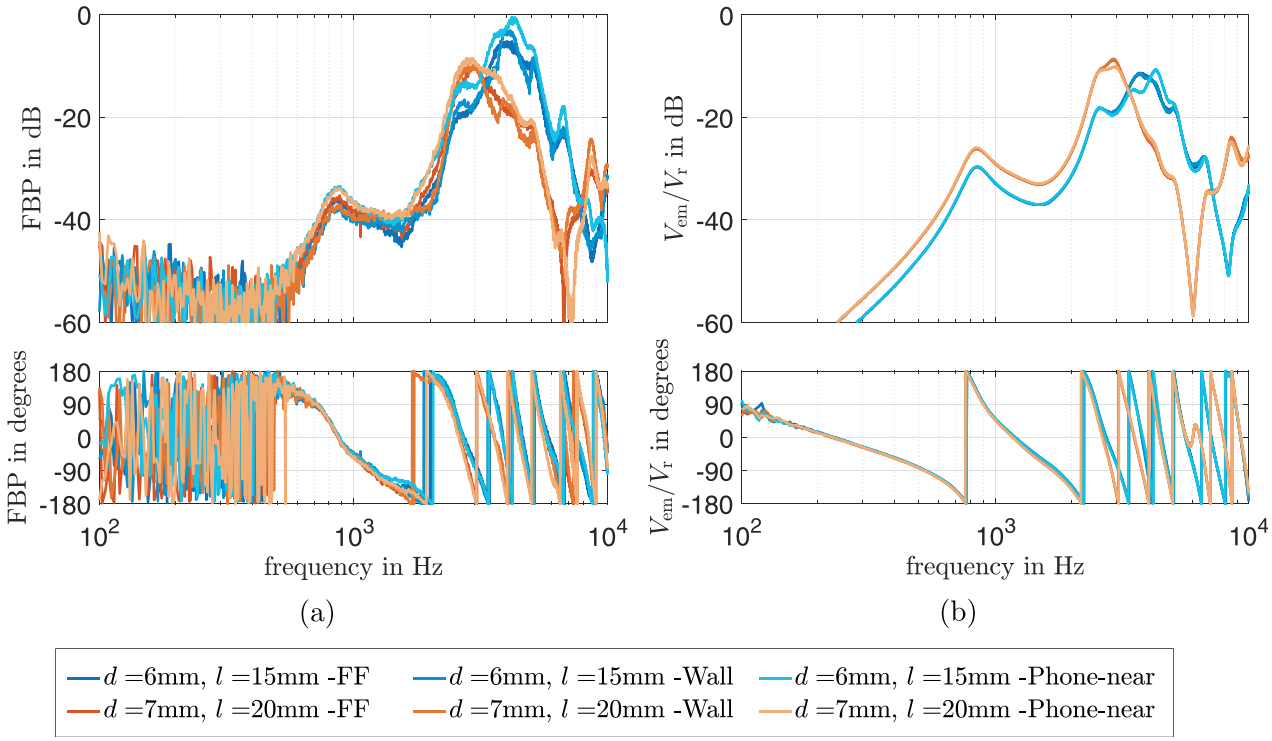

FIG. 7. (Color online) (a) Acoustic feedback paths (defined as V_m/V_r) and (b) transfer function of the ear canal microphone relative to the receiver voltage V_{em}/V_r measured using a BTE hearing aid on a dummy head with variable ear canals for different sound field conditions and ear canal geometries.

measured in the free-field ($M = 2$) condition were used (DFD ee and DFD wee) and (2) all acoustic feedback paths ($M = 6$), i.e., free-field, wall, and telephone were used (DFD ee full and DFD wee full).

3. Parameters of the feedback path model based on a defined physical location for the decomposition

The filter coefficients in Eqs. (28) and (29) of the fixed part variants A and B, respectively, as well as the coefficients of variant C for the fixed part (cf. Sec. III C) were derived using the iterative procedure according to Steiglitz and McBride (1965), using five iterations. For all three variants (A, B, and C), the coefficients were computed for $N_p, N_z \in [0, 1, 2, \ldots, 30]$.

C. Comparison of the fixed part variants based on a defined physical location for the decomposition

The fixed parts according to the variants A and B estimate $Q_v B_m/V_r$, i.e., the volume velocity out of the vent multiplied by the sensitivity of the hearing aid microphone divided by the voltage driving the receiver. The fixed part in variant C estimates V_{em}/V_r, i.e., the voltage at the ear canal microphone relative to the receiver voltage. Thus, the three variants cannot be compared directly. The volume velocity cannot be measured without causing additional errors. This means the true fixed part for the variants A and B is in principle unknown. However, the parametrization of the transfer functions can be compared in variants A and B, i.e., comparing the desired fixed part given by Eq. (16) with H_A^f and H_B^f given by Eqs. (28) and (29).

In the left panel of Fig. 8 the fixed parts according to the variants A and B can be seen for the feedback path measured on the large ear canal under free-field condition using $N^f = 20$ parameters. Additionally, the desired transfer function of the fixed part is shown which results from the non-parameterized feedback path according to Eq. (16). For both variants the highest accuracy is reached in the frequency range where the transfer function has its maximum. This is a characteristic of the fitting procedure according to Steiglitz and McBride (1965), which is a desired effect here. Variant A shows much larger deviations to the desired transfer function of the fixed part for frequencies below 1.5 kHz compared to variant B. This is due to the fact that in variant A only 14 parameters of the $N^f = 20$ parameters are used for the pole-zero filter of the fixed part, while in variant B all 20 parameters are used for the pole-zero filter. On the other hand variant A shows a better agreement than variant B at high frequencies where the desired transfer function has its minimum.

The desired (V_{em}/V_r) and the parametrized transfer function of the fixed part of variant C are shown in the right panel of Fig. 8. Similarly to the other variants, a very good agreement can be seen in a broad frequency range around the maximum of the transfer function. For frequencies below 1 kHz and at the minimum at about 8 kHz large deviations can be seen.

D. Comparison of feedback path models

Figure 9 shows in the left column the measured and the estimated complete feedback path using the three variants

https://doi.org/10.1121/10.0000509

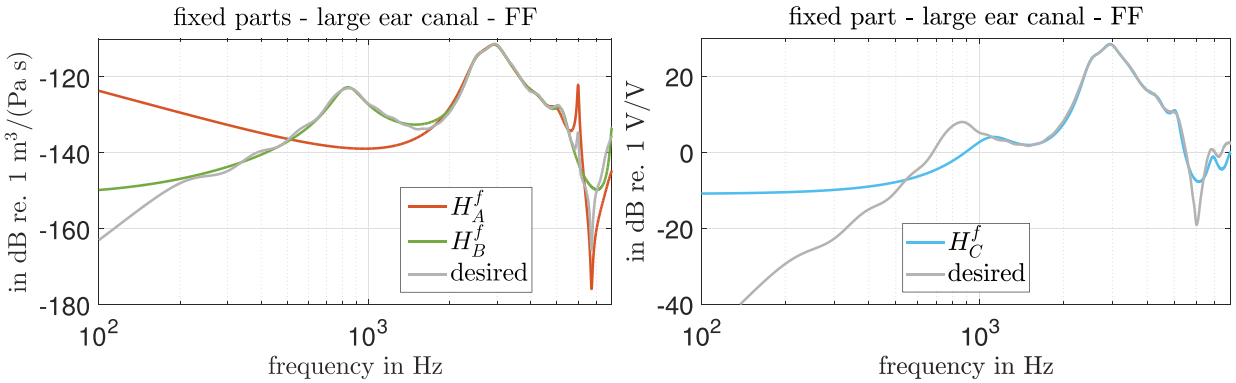

FIG. 8. (Color online) Example of the different fixed part variants ($N^f = 20$) for the large ear canal and the free-field condition.

based on a defined physical location (DPL A, DPL B, DPL C) for the large ear canal and the free-field condition. The right column shows the deviations of the estimated to the measured feedback path. The estimations of all variants show a very good agreement with the measurement for the important frequency range around the maximum of the feedback path. At lower and at higher frequencies larger deviations from the measured feedback path as well es differences between the variants can be observed. However, it can be assumed that these deviations do not affect feedback cancellation due to the limited maximum output of the speaker at these frequencies.

While it is difficult to assess the performance of the different variants based on Fig. 9, in this section all feedback path models are compared in terms of the added stable gain. In all models described in previously, the achieved ASG depends on both, the number of parameters of the fixed part and that of the variable part. In order to compare the different models an exemplary number of fixed part parameters $N^f = 20$ was chosen. Note that for the DFD models, different combinations of poles and zeros can result in the same number of fixed parameters, we show the results of those combinations that resulted in the largest ASG, which may be different for different N^v. Figure 10 shows the ASG for the free-field condition and the large ear canal for each model as a function of N^v. For values of $N^v \leq 10$ a large increase of the ASG with N^v can be observed for all models. From about $N^v = 10$ this increase is slightly smaller and from about $N^v = 30$ is very small.

The largest ASGs were achieved by the DFD wee model followed by the DFD ee model which are both based

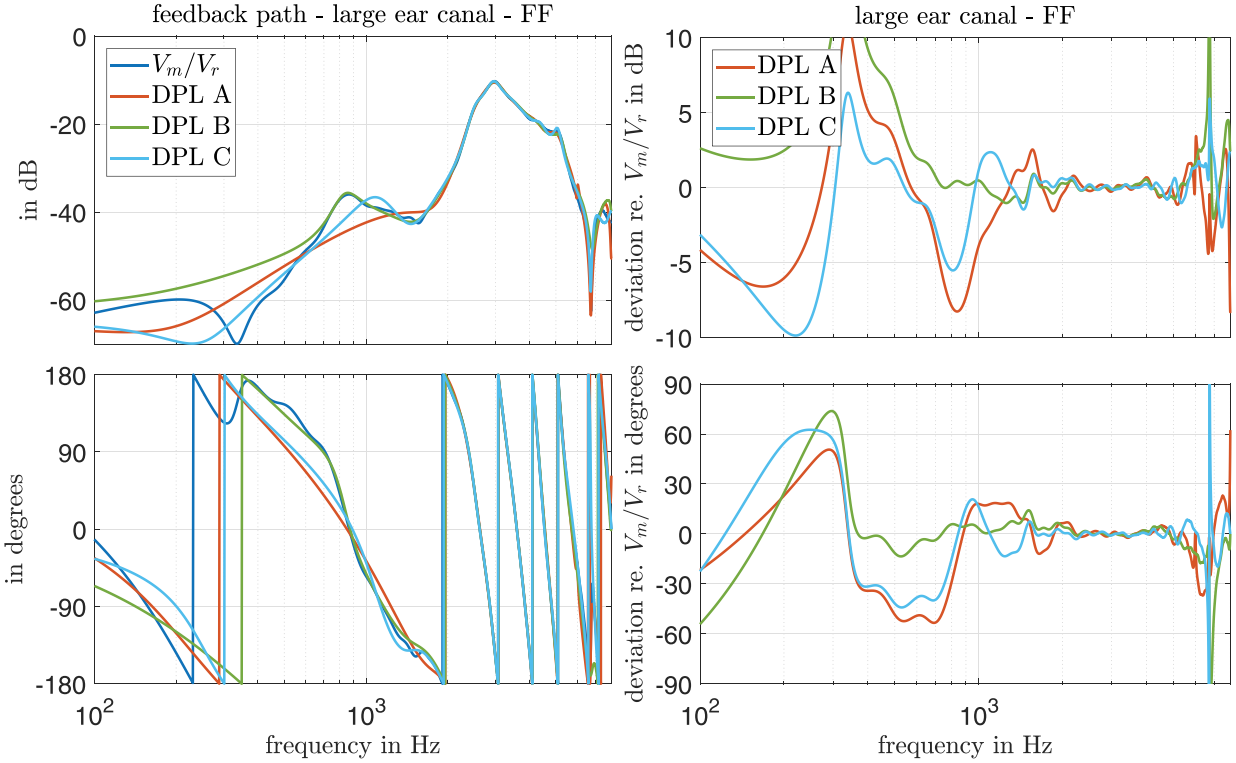

FIG. 9. (Color online) Left: Feedback paths for the large ear canal and the free-field condition, measurement and estimations with the combined feedback path models using the different fixed part variants ($N^f = 20$, $N^v = 20$). Right: Deviation of the estimated relative to the measured feedback path.

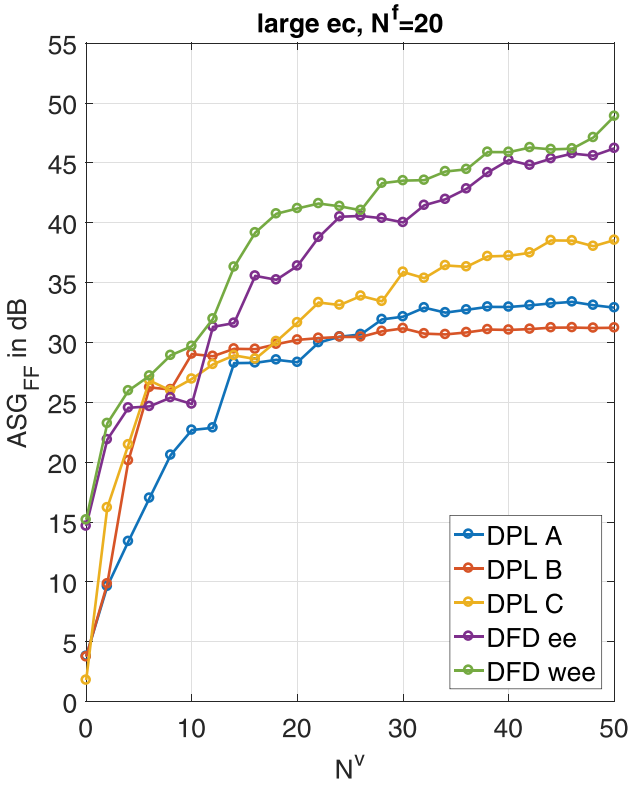

FIG. 10. (Color online) Added stable gain as a function of N^v with $N^f = 20$ for the large ear canal and the free-field condition for all models.

on digital filter design. The models based on a defined physical location achieve significantly smaller values of ASG for $N^v > 10$. For $N^v \geq 20$ the variant C outperforms the variants A and B. While these results show the potential of the different models, they do not allow one to draw conclusions about the generalizability and robustness, see discussion in Secs. V A and V B.

In order to compare the performance of all models for both ear canals and all environmental condition, Fig. 11 shows the median and quartiles of the ASG values in the range of $10 \leq N^v \leq 30$ for each combination of model, ear canal, and environmental condition. The left panel of Fig. 11 shows the results for the free-field condition. As can be observed the digital filter design based models using only the free-field measurement for optimization (DFD ee and DFD wee) achieve the largest ASG values for the smaller ear canal as well as for the larger ear canal. As can be expected when increasing the set of acoustic feedback paths included in the optimization, the ASG values for the DFD ee full and DFD wee full models are generally lower in the free-field condition. For the other environmental conditions the performance of the different approaches changes. For both, the wall (middle panel of Fig. 11) and the telephone condition (Fig. 11) the models based on a defined physical location achieve significantly better ASG values compared to the models based on digital filter design that used only the free-field measurements for optimization (DFD ee and DFD wee). When using all measurements for optimization, however, the performance of the models based on digital filter design is comparable to the performance of the models based on a defined physical location. Generally, among the models based on a defined physical location there is no clear difference between the variants. However, note that for the small ear canal a trend of better ASG values with variant C compared to variants A and B can be observed. Comparing the models based on digital filter design the DFD wee and DFD wee full models achieve better values of the ASG than the DFD ee and DFD ee full models.

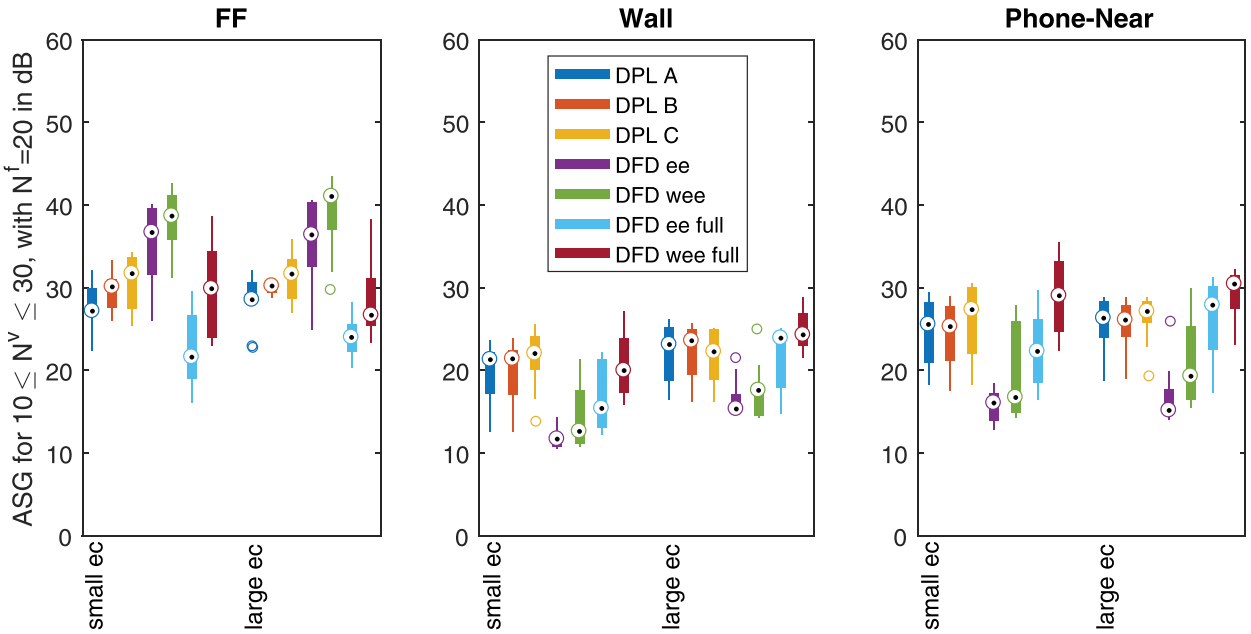

FIG. 11. (Color online) Results of the added stable gain for $10 \leq N^v \leq 30$ with $N^f = 20$ for each model and each ear canal. Results are shown on the left for the free-field condition, in the middle for the condition next to a wall, and on the right for the telephone condition.

https://doi.org/10.1121/10.0000509

V. DISCUSSION

A. Practical considerations and robustness

Two different approaches have been presented to decompose the acoustic feedback path(s) into a time-invariant fixed part and time-varying variable part(s) either using a model based on a defined physical location or based on digital filter design. Both of these modeling approaches provide (mostly) complementary advantages and disadvantages.

On the one hand, the model based on a defined physical location for the decomposition requires an additional microphone in the ear canal and knowledge of the microphone sensitivities. Using the additional microphone, the effort to fit the acoustic feedback path model can be kept small, requiring only a single measurement on the subject, which is similar to fitting procedures of feedback cancellation system of commercially available hearing aids. Furthermore, the model based on a defined physical location is able to provide a fixed part that generalizes well across different acoustic feedback paths.

On the other hand, the model based on digital filter design does not require an additional microphone and can thus be applied to any hearing aid, e.g., in this study a BTE hearing aid with two microphones, which is the case for most commercially available hearing aids. While the measurement of the acoustic feedback paths can be performed in a comparable amount of time that is used to fit acoustic feedback cancellation system in commercially available hearing aids, the fixed part obtained using a single measurement is not as robust to changes in the acoustic feedback paths as the fixed part obtained from the model based on a defined physical location for the decomposition. However, the robustness of the fixed part obtained by using digital filter optimization to variations can be significantly increased by using multiple feedback path measurements in the optimization (e.g., when the acoustic feedback path is measured in different acoustic conditions as used in the ee full and wee full models). Nevertheless, this requires a careful choice of the acoustic conditions included in the different feedback path measurements. Note that in this study, we have included a free-field, a wall and a telephone condition which covered a broad variability, hence, even though evaluations were carried out using the same measurements, it is expected, that the robustness to unknown feedback paths is similar.

In conclusion, both modeling approaches provide a trade-off between suitability to a specific hearing aid design combined with robustness to variations and the independence of the hearing aid design combined with an increased effort during fitting to achieve robustness.

B. Number of parameters

In all considered approaches the feedback path is modeled with a fixed part and a variable part. In order to ensure a fast adaptation of the feedback canceler to a changing feedback path, the number of parameters of the variable part should be small. However, if the number of parameters of the variable part is too small, variations of the feedback path cannot be captured, i.e., the ASG decreases. Furthermore, the number of parameters of the fixed part should not be too large in order to avoid overfitting.

A detailed evaluation addressing the optimal order of the models is beyond the scope of this paper, however, Fig. 12 shows the ASG as a function of the number of fixed parameters for a constant number of both, fixed part and variable part parameters of $N = 40$.

A desired property of the modeling of the fixed part is to reduce the number of variable part parameters while maintaining a high ASG, i.e., having results that are in the top right corner in Fig. 12. As can be seen for a number of up to 20 parameters for the fixed part (N^f), the performance of the two different models is very similar. For the small ear canal the ASG is in the range of 20 to 35 dB and for the large ear canal the ASG is in the range of 22 to 37 dB. If N^f is increased further (i.e., the numbers of parameters of the variable part N^v is decreased), the ASG decreases for the combined model with variant C of the fixed part. With the DFD wee full model based on digital filter design the ASG only slightly decreases or even remains constant for N^f between 20 and 30. Hence, when aiming to reduce the number of variable part parameters, the DFD wee model leads to the best results. However, note that especially for larger $N_f > 20$, the presented results need to be interpreted with care since in contrast to the DPL model all feedback paths were known during the optimization. While the DFD model is expected to result in slightly lower ASG values for unknown feedback paths compared to the known feedback paths, results in (Schepker and Doclo, 2016b) suggest that the performance can still be considered similar. In conclusion, both models are able to reduce the number of variable part parameters, which in a practical implementation may lead to an increased convergence speed of an adaptive filter as has been shown in Schepker and Doclo (2016a,b).

C. Difference in model structure to Ma *et al.* (2011)

The decomposition of the acoustic feedback path in hearing aids into a fixed part and a variable part was first proposed by Kates (2000) and recently extended in Ma *et al.* (2011) and Schepker and Doclo (2014). Ma *et al.* (2011) argued that, in contrast to models based on digital filter design, pure electro-acoustic models of the acoustic feedback could not provide the necessary modeling accuracy. However, as shown in this study, models based on a defined physical location for the decomposition, including electro-acoustic models, can be used to obtain a good estimate of the fixed part which can provide a significant increase in the robustness of the estimated acoustic feedback path towards unknown variants that may occur in everyday use.

Furthermore, Ma *et al.* (2011) assumed that the fixed part models only hearing aid specific parts. This is in contrast to the present study, where patient specific characteristics, i.e.,

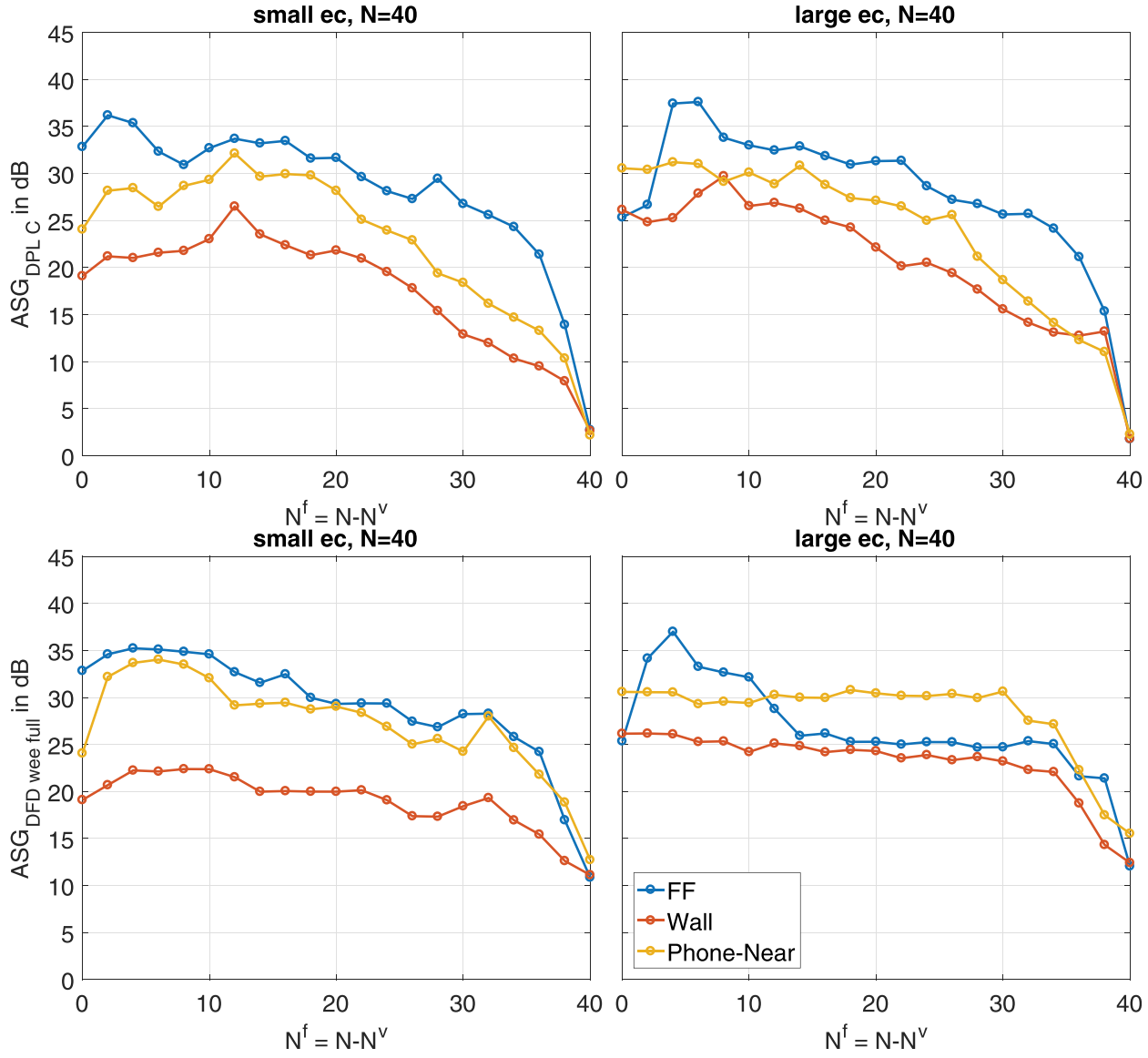

FIG. 12. (Color online) Results of the added stable gain for a constant $N = 40$ for the combined model with variant C (top) and for the model wee full (bottom). The left column shows results for the small ear canal and the right column results of the large ear canal. The different colors indicate the different environmental conditions.

properties of the acoustic feedback path due to the individual anatomy of the patients' ears, are included in the fixed part of the acoustic feedback path model. When using the model based on a defined physical location for the decomposition, these patient specific characteristics are explicitly included, while for the model based on digital filter optimization these are included by the choice of the set of measurements that is used to optimize the fixed and variable parts.

In order to compare the effects of a patient specific fixed filter and a hearing aid specific filter, Fig. 13 shows the results for the model based on digital filter optimization when different sets of acoustic feedback paths are used in the optimization. In addition to the previously compared models we also include the following models.

(1) DFD non-independent (non-ind.) ee and the DFD non-ind. wee model, where we used the free-field measurements of both ear canal configurations, i.e., a total of $M = 4$ measurements, to obtain a patient independent and hearing aid specific fixed part. Note that by the choice of the measurements, these models can be considered to provide average models across two ear canal geometries.
(2) DFD ee half and DFD wee half, where for each ear canal setting we used the free-field and phone-near measurements, i.e., a total of $M = 4$ measurements, to obtain patient-specific fixed parts.

These models allow one to compare the effects of a patient-specific fixed filter and a hearing aid specific fixed filter using the same number of measurements used in the optimization of the fixed filter. Note that for both settings the wall condition was not included in the optimization and thus provides insight into the robustness of the fixed part. In general, for the free-field and phone-near conditions the

https://doi.org/10.1121/10.0000509

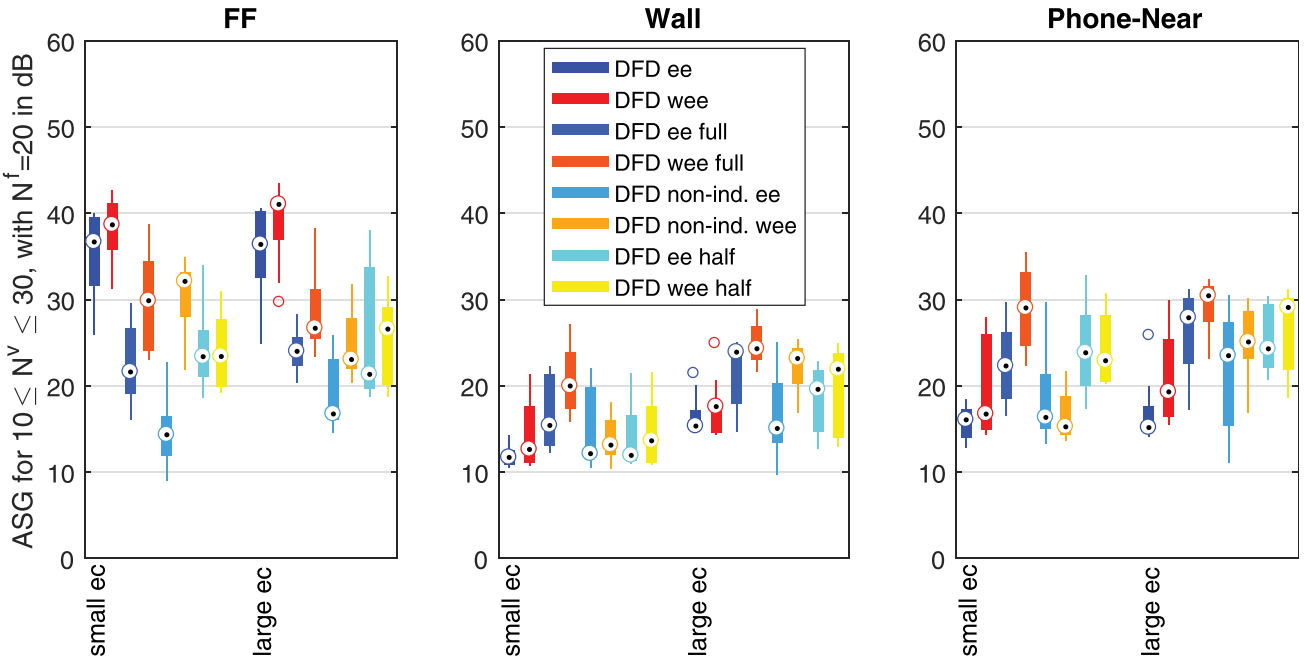

FIG. 13. (Color online) Results of the added stable gain for $10 \leq N^v \leq 30$ with $N^f = 20$ for the DFD-models with and without individualization for each ear canal. Results are shown for the free-field condition (left), for the condition next to a wall (center), and for the telephone condition (right).

assumptions of a patient-specific fixed filter leads to larger ASG. For the wall condition, the results indicate that depending on the used optimization procedure a similar or better median performance is obtained for the patient-specific fixed part compared to a hearing aid-specific fixed part.

In practice, generally the lowest ASG across different acoustic conditions determines the amount of amplification that can be applied in a hearing aid. For the results in Fig. 13 the lowest median ASGs for the different models are 12 dB (DFD non-ind. ee), 13 dB (DFD non-ind. wee), 12 dB (DFD ee half), and 14 dB (DFD wee half) for the smaller ear canal, as well as 15 dB (DFD non-ind. ee), 23 dB (DFD non-ind. wee), 20 dB (DFD ee half), and 22 dB (DFD wee half) for the large ear canal. Again, this analysis shows that depending on the used optimization procedure, the patient-specific fixed part performs better or at least as well as the hearing aid specific fixed part.

VI. CONCLUSION

In this paper, acoustic feedback path models were investigated where the acoustic feedback path was decomposed into two different filters: (1) a time-invariant *fixed part* and (2) a time varying *variable part*. Two different approaches used to model the fixed part were compared, both using signals from at least two microphones: (1) a digital filter design approach using an existing acoustic feedback path model which makes use of at least two measurements, e.g., from the two microphones in a two-microphone hearing aid and (2) a defined physical location approach that exploits a novel electro-acoustic model of a hearing aid as well as the signals of one hearing aid microphone and an additional ear canal microphone. The performance of both approaches was investigated using measured feedback paths from a two-microphone behind-the-ear hearing aid with an additional ear canal microphone.

It was shown that both approaches yield comparable results in terms of the average ASG. In order to compute a fixed part model that allows for a robust performance with different unknown acoustic feedback paths, both approaches provide a trade-off between the requirement of an ear canal microphone and a minimal effort during hearing aid fitting for the physical-location-based model on the one hand, and the independence of the hearing aid design and an increased effort during fitting for the digital filter-design-based model on the other hand. A comparison of the performance for a constant total number of parameters ($N = 40$) using the best variants of both approaches showed that both models are able to reduce the number of variable part parameters while maintaining a high ASG and therefore potentially allow for an increased convergence speed of an adaptive filter, as has been shown in Schepker and Doclo (2016a,b). Furthermore, a comparison between a hearing aid-specific fixed part and the proposed patient-specific fixed part showed the potential of using a patient-specific fixed part.

ACKNOWLEDGMENTS

This work was funded by the Deutsche Forschungsgemeinschaft (DFG, German Research Foundation)—project number 352015383—SFB 1330 C1, the Research Unit FOR 1732 "Individualized Hearing Acoustics" and the Cluster of Excellence 1077 "Hearing4All."

Benade, A. H. (**1968**). "On the propagation of sound waves in a cylindrical conduit," J. Acoust. Soc. Am. **44**(2), 616–623.

Blau, M., Sankowsky, T., Roeske, P., and Fischer, S. (**2009**). "Predicting the acoustics of individual ears for hearing aid and audio applications—Model framework and future work," in *Proceedings of NAG/DAGA 2009*, Rotterdam, the Netherlands, pp. 1266–1268.

Blau, M., Sankowsky, T., Stirnemann, A., Oberdanner, H., and Schmidt, N. (**2008**). "Acoustics of open fittings," in *Proceedings of Acoustics '08*, Paris, pp. 711–716.

Egolf, D. P., Haley, B. T., Howell, H. C., Legowski, S., and Larson, V. D. (**1989**). "Simulating the open-loop transfer function as a means for understanding acoustic feedback in hearing aids," J. Acoust Soc. Am. **85**(1), 454–467.

Egolf, D. P., Howell, H. C., Weaver, K. A., and Barker, D. S. (**1985**). "The hearing aid feedback path: Mathematical simulations and experimental verification," J. Acoust. Soc. Am. **78**(5), 1578–1587.

Giri, R., and Zhang, T. (**2017**). "Bayesian blind deconvolution with application to acoustic feedback path modeling," in *IEEE International Conference on Acoustics, Speech, and Signal Processing (ICASSP)*, New Orleans (March 2017), pp. 601–605.

Guo, M., Jensen, S. H., and Jensen, J. (**2012**). "Novel acoustic feedback cancellation approaches in hearing aid applications using probe noise and probe noise enhancement," IEEE Trans. Audio Speech Lang. Process. **20**(9), 2549–2563.

Hashemgeloogerdi, S., and Bocko, M. F. (**2018**). "Inherently stable weighted least-squares estimation of common acoustical poles with the application in feedback path modeling utilizing a Kautz filter," IEEE Sign. Process. Lett. **25**(3), 368–372.

Hellgren, J., Lunner, T., and Arlinger, S. (**1999**). "Variations in the feedback of hearing aids," J. Acoust. Soc. Am. **106**(5), 2821–2833.

Hiipakka, M., Tikander, M., and Karjalainen, M. (**2010**). "Modeling the external ear acoustics for insert headphone usage," J. Audio Eng. Soc. **58**(4), 269–281.

Kates, J. M. (**1988**). "A computer simulation of hearing aid response and the effects of ear canal size," J. Acoust. Soc. Am. **83**(5), 1952–1963.

Kates, J. M. (**2000**). "Feedback cancellation apparatus and methods," U.S. patent 6,072,884.

Kates, J. M. (**2001**). "Room reverberation effects in hearing aid feedback cancellation," J. Acoust. Soc. Am. **109**(1), 367–378.

Ma, G., Gran, F., Jacobsen, F., and Agerkvist, F. (**2011**). "Extracting the invariant model from feedback paths of digital hearing aids," J. Acoust. Soc. Am. **130**(1), 350–363.

Nakagawa, C. R. C., Nordholm, S., and Yan, W.-Y. (**2015**). "Analysis of two microphone method for feedback cancellation," IEEE Sign. Process. Lett. **22**(1), 35–39.

Sankowsky-Rothe, T., and Blau, M. (**2017**). "Static and dynamic measurements of the acoustic feedback path of hearing aids on human subjects," Proc. Mtgs. Acoust. **30**(1), 050008.

Sankowsky-Rothe, T., Blau, M., Köhler, S., and Stirnemann, A. (**2015a**). "Individual equalization of hearing aids with integrated ear canal microphones," Acta Acust. Acust. **101**(3), 552–566.

Sankowsky-Rothe, T., Blau, M., Schepker, H., and Doclo, S. (**2015b**). "Reciprocal measurement of acoustic feedback paths in hearing aids," J. Acoust. Soc. Am. **138**(4), EL399–EL404.

Sayed, A. (**2003**). *Fundamentals of Adaptive Filtering* (Wiley, Hoboken, NJ).

Schepker, H., and Doclo, S. (**2014**). "Modeling the common part of acoustic feedback paths in hearing aids using a pole-zero model," in *Proceedings of the IEEE International Conference on Acoustics, Speech and Signal Processing (ICASSP)*, Florence, Italy, pp. 3693–3697.

Schepker, H., and Doclo, S. (**2015**). "Common part estimation of acoustic feedback paths in hearing aids optimizing maximum stable gain," in *Proceedings of the IEEE International Conference on Acoustics, Speech and Signal Processing (ICASSP)*, Brisbane, Australia, pp. 649–653.

Schepker, H., and Doclo, S. (**2016a**). "Estimating the common pole-zero model of acoustic feedback paths in hearing aids using semidefinite programming," IEEE Trans. Audio Speech Lang. Process. **24**(2), 366–377.

Schepker, H., and Doclo, S. (**2016b**). "Least-squares estimation of the common pole-zero model of acoustic feedback paths in hearing aids," IEEE Trans. Audio Speech Lang. Process. **24**(8), 1334–1347.

Schepker, H., Tran, L. T. T., Nordholm, S., and Doclo, S. (**2016**). "Improving adaptive feedback cancellation in hearing aids using an affine combination of filters," in *Proceedings of the IEEE International Conference on Acoustics, Speech and Signal Processing (ICASSP)*, Shanghai, China (March 2016), pp. 231–235.

Spriet, A., Doclo, S., Moonen, M., and Wouters, J. (**2008**). "Feedback control in hearing aids," in *Springer Handbook of Speech Processing*, edited by J. Benesty, M. M. Sondhi, and Y. Huang (Springer, Berlin), pp. 979–999.

Steiglitz, K., and McBride, L. (**1965**). "A technique for the identification of linear systems," IEEE Trans. Auto. Control **10**(4), 461–464.

Stinson, M. R., and Daigle, G. A. (**2007**). "Transverse pressure distributions in a simple model ear canal occluded by a hearing aid test fixture," J. Acoust. Soc. Am. **121**(6), 3689–3702.

Strutt, J. W. (Lord Rayleigh) (**1896**). *The Theory of Sound* (Macmillan, London), Vol. 2.

van Waterschoot, T., and Moonen, M. (**2011**). "Fifty years of acoustic feedback control: State of the art and future challenges," Proc. IEEE **99**(2), 288–327.